Kustaanheimo-Stiefel variables for planetary protection compliance analysis

A. Masat*, M. Romano† and C. Colombo ‡
Polythecnic University of Milan, Milan, Italy, 20156

Planetary protection in trajectory design aims to assess the impact probability of space mission disposed objects based on their initial uncertain conditions, to avoid contaminating other planetary environments. High precision dynamical models and propagation methods are required to reach high confidence levels on small estimated impact probabilities. These requirements have so far confined planetary protection analyses to robust Monte Carlo-based approaches, using the Cartesian formulation of the full force problem dynamics. This work presents the improvements brought by adopting the Kustaanheimo-Stiefel (KS) formulation of the dynamics. The KS formulation is combined with reference frame switch procedures and adaptive non-dimensionalization upon detection of close encounters. The fibration property of the KS space, namely the parametrizable locus of point arising when mapping to a higherdimensional space, is exploited to minimize the computational time, because of the minimized numerical stiffness of the system. Impact probability estimation tasks become more efficient than the single simulation case, since the regularization of the dynamics removes the singularity of gravitational potentials for distances approaching zero. Despite an almost halved computational burden for Monte-Carlo analysis, the precision of the single simulations is increased by nearly one order of magnitude, setting a new performance benchmark for planetary protection tasks.

*PhD Candidate, DAER - Department of Aerospace Science and Technology, Via G. La Masa 34, Milano, Italy, alessandro.masat@polimi.it
†Postdoctoral researcher, DAER - Department of Aerospace Science and Technology, Via G. La Masa 34, Milano, Italy, matteo1.romano@polimi.it
‡Associate Professor, DAER - Department of Aerospace Science and Technology, Via G. La Masa 34, Milano, Italy, camilla.colombo@polimi.it

Nomenclature

(i, j, k)	=	Unit vectors of the Cartesian frame
$\underline{r} = \{r_1, r_2, r_3\}^T$	=	Cartesian position vector
$\mathbf{r}$	=	Quaternion with vanishing k component of the position vector $\underline{r}$
r	=	Magnitude of $\mathbf{r}$ or $\underline{r}$
$\mathbf{u} = \{u_1, u_2, u_3, u_4\}^T$	=	KS quaternion
$\overline{\mathbf{u}}$	=	Conjugate of $\mathbf{u}$
$\mathbf{u}^*$	=	Star-conjugate (anti-involute) of $\mathbf{u}$
φ	=	Angle parametrizing the fibration of the KS space
$\mathbf{L}(\mathbf{u})$	=	Multiplication matrix of the KS1 transform
s	=	Fictitious KS time
t	=	Physical time
$\frac{d(\cdot)}{dt}$ or $\dot{(\cdot)}$	=	First derivative with respect to t
$\frac{d^2(\cdot)}{dt^2}$ or $\ddot{(\cdot)}$	=	Second derivative with respect to t
$\frac{d(\cdot)}{ds}$ or $(\cdot)'$	=	First derivatives with respect to s
$\frac{d^2(\cdot)}{ds^2}$ or $(\cdot)''$	=	Second derivatives with respect to s
β	=	Arbitrary constant for the Sundman transformation
K	=	Arbitrary function of position, time and velocity for the Sundman transformation
ϵ	=	Kepler orbital energy
ϵ_0	=	Total orbital energy
μ	=	Gravitational parameter of the primary body in the Kepler problem
$\underline{f}(\underline{r}, t)$	=	Generic perturbation in Cartesian coordinates, function of $\underline{r}$ and t
$\mathbf{f}(\mathbf{r}, t)$	=	$\underline{f}$ written as quaternion with vanishing k component
n, N	=	body identifier and limit of the restricted N-body problem
μ_n	=	gravitational parameter of body n
$\mathbf{r}_n$	=	Cartesian position of body n written as quaternion with vanishing k component

$\{l_{ref}, t_{ref}, v_{ref}, \mu ref\}$	=	reference dimensional length, physical time, velocity, gravitational parameter
$\{AU, Year\}$	=	Astronomical Unit and Year
$(\mathbf{p}, p_l, p_m,)$	=	Condensed for linear combination of KS states
(δ, ν)	=	Displacements along the fibration parameter φ
EN	=	abbreviation for Energetic non-dimensionalization
AUY	=	abbreviation for AU-Year non-dimensionalization
FIXED	=	abbreviation for integration without frame switch
SWITCH	=	abbreviation for integration with frame switch
SUN	=	abbreviation for Sun-centric interplanetary simulations
SSB	=	abbreviation for barycentric interplanetary simulations
RK45	=	Runge Kutta 4(5) integration scheme
RK78	=	Runge Kutta 7(8) integration scheme
SolO	=	Solar Orbiter

I. Introduction

Complying with planetary protection policies introduces a set of technical requirements that any space mission phase or task must contribute to fulfil. In order not to contaminate the environment of any visited planet, care must be taken particularly for those objects which cannot be sterilized because of their function, such as upper stages of launchers. For instance, a mission to Mars has all of its lander components sterilized before launch, so that possible traces of life are not introduced from Earth, but the stages of the launchers are not and cannot be. Furthermore, they are disposed in space once the injection of the payload into its route to Mars is completed, which makes their dynamics completely uncontrolled. Planetary protection policies are developed and maintained every few years by COSPAR (Committe On Space Research) [1]. The work of Kminek et al. [2] outlines the requirements that any European Space Agency's (ESA) mission must fulfill. For disposal objects they turn into body-dependent small values of accepted impact probability (lower for higher likelihood to find traces of local life in the specific moon or planet), which must be estimated at 95% confidence level and considering the evolution of the uncontrolled trajectory 100 years forward in time.

Starting from the requirements introduced by Kminek et al. [2], the ESA SNAPPshot suite was developed by Letizia et al. [3, 4] and Colombo et al. [5] to compute the impact probability of a given initial condition and uncertainty. A

Monte Carlo simulation is performed on a large set of trajectory propagations, computed in the Cartesian formulation of the full force dynamics, keeping static reference frame and non-dimensionalization quantities throughout the integration. The impact probability of the orbiting body with all the planets encountered in the trajectory is then determined as the ratio between the number of runs turning into an impact over the total number of generated samples.

Romano et al. [6] proposed a line sampling method for the computation of impact probabilities. It is a Markov Chain Monte Carlo-based approach, which bounds the uncertainty regions finding the lines perpendicular to such regions, and therefore sampling the uncertainty along them. It ensures a better estimate especially for small probabilities and is also more efficient, as it requires around 35% less total runs than the standard Monte Carlo. Another work from Romano [7] investigated the influence of numerical schemes in the performance and precision of the SNAPPshot [5] approach. An attempt was also made to develop a covariance propagation technique in the Cartesian formulation of the dynamics, motivating the choice of regularized formulation of this work. Even before flyby events, the propagated continuous covariance quickly degrades when Cartesian dynamics is used because of the strong non-linearity and the Lyapunov instability of the Kepler problem, requiring to split the uncertainty initial distribution repeatedly and cumulatively [7]. The results obtained in [7], together with other functionalities, contributed to the development of the improved version of the SNAPPshot suite [8].

Regularizing the dynamics is not necessarily attached to a new set of coordinates per se, in fact the Kustaanheimo-Stiefel (KS) regularization was born bringing together two concepts: the first, adding a fourth coordinate trying to describe the Kepler problem as a four dimensional harmonic oscillator, originally presented by Kustaanheimo [9], and the introduction of the time transformation of the Sundman type [10], operated later with the contribution of Stiefel [11]. All the later developments over the newly created KS formalism use to refer to the more comprehensive manuscript by Stiefel and Scheifele [12]. Bond proposed a variation of parameters approach that generically accounts for perturbing effects starting from the original four-vector KS formulation [13].

In the work of Stiefel and Scheifele [12] the properties of quaternion algebra are mentioned, even though the original developers of the KS transformation did not pay much attention on this aspect. Quaternions in the KS formalism have been explored first by Velte [14] and better detailed by the successive works of Vivarelli [15–17], introducing the concept of anti-involute and quaternion cross product. The KS transformation was re-derived and refined in the quaternion formalism by Deprit et al. [18] where it was obtained by doubling from a Levi-Civita transformation. Deprit [19–21] also extensively studied the canonical Lissajous transformation, concept that has recently been re-proposed by Breiter and Langner [22, 23] starting from the KS formulation. A more recent work by Waldvogel [24] provided new insight on the algebraic properties of quaternions in the KS regularization and the related fibration of the KS space, re-defining Vivarelli's anti involute [16] as the quaternion star conjugate.

Saha [25] proposed a quaternion approach to the KS transformation more suitable to the analysis of Hamiltonian systems. Based on the work of Saha, Breiter and Langner [26] explored the role of the preferential direction chosen to

perform the regularization, which they generalized to an arbitrary one of the original three-dimensional space. In fact, almost all the analyses already performed in the context of the KS formulation adhere to the original one proposed by Kustaanheimo and Stiefel [11]. Denoting with (x, y, z) the axes of a generic three-dimensional Cartesian space, not necessarily attached to any commonly used Solar System direction, the first coordinate x was selected as the reference direction for the KS transformation. Using the same notation as Breiter and Langner [26], choosing x as preferential direction the KS tranformation is identified as KS1, whereas for instance the KS3 version is presented by Saha [25] using the direction z. The work of Breiter and Langner [26] did not stop to this generalization, but provided new insight to the physical meanings of the KS coordinates themselves.

Partially quoting Breiter and Langner [26] and recalling the quaternion description of rotations, in the KS1 version "the normalized KS variables are the Euler-Rodrigues parameters of the rotation turning the x axis into the direction of the Cartesian position vector which generated the KS coordinates". From this sentence, the physical meaning of the fibration property of the transformation [12, 24, 26] also becomes more clear, recalling that such a rotation may happen in an infinite number of ways. Another work by Langner and Breiter [27] explores the properties of the quaternionic KS formulation in Hamiltonian systems, tackling also the rotating frame case. Some other work in a similar direction was done by Roa and Peláez [28], they make use of the Minkowskian geometry that was originally proposed by Kustaanheimo and Stiefel [9, 11] to handle close approaches and their hyperbolic geometry. Still Roa et al. also worked on the KS formulation [29], showing that the Lyapunov stability does not apply to the whole KS fiber with respect to the physical time. Roa and Kasdin made use of quaternions also developing a new set of non-singular orbital elements that models the intermediary evolution of the orbital plane [30].

When dealing with regularized orbital dynamics, the DROMO formulation is among the latest state-of-the-art results for the perturbed two-body problem. It was first proposed by Peláez et al. [31], seeking for a numerically stable, regularized and efficient formulation, furthermore rendering the same accurate results for any type of primarily two-body trajectory (elliptical, parabolic, hyperbolic) [32], using a variation of parameters approach. The description of the motion is broken into three steps [32]: the evolution of the orbital plane, the evolution of the trajectory on the orbital plane and finally the position change on the osculating orbit as a function of time. The independent variable is a fictitious time obtained by a Sundman transformation [10], which reduces to the true anomaly in case of Keplerian motion, instead of the eccentric anomaly of the KS case. The original DROMO formulation is singular for null angular momentum. Recent revisions worked to fix these sensitivity issues: Baù et al. [33] developed E-DROMO, a non-singular formulation of DROMO for any bound orbit, removing the singularities on null eccentricity and inclination. Roa et al. [34] analyzed the singularities posed by deep flybys and then proposed the re-formulation H-DROMO, not sensitive to a vanishing angular momentum. The latest updates involve the study of the evolution of an intermediate frame [35]. The interest on universal variables, capable of managing either closed, open or even rectilinear trajectories is introduced. Amato et al. [36] studied the reference frame switch for close approaches using the DROMO formulation, and numerically

identified a region of "best switch distance" that does not correspond either to the Hill surfaces or the sphere of influence. The way all the DROMO formulations were built makes them sensitive to the task they are used for. In the case of flyby events, a frame switch procedure is required to enhance its robustness, being a variations of parameters approach. Moreover, if events need to be computed requiring to retrieve the propagated coordinates, the conversion burden is inevitably added to the integration runtime, although DROMO, and variations of parameters in general, remain more efficient in terms of accuracy and required function evaluations. Furthermore, the DROMO approach remains limited to the perturbed two-body problem. KS coordinates are chosen because of the introduction of the barycentric version in this work, foreseeing a future validation of the technique to low-energy planetary protection tasks, building a framework conceptually similar to the rotating frame case proposed by Langner and Breiter [27]. A new term appears in the KS Hamiltonian in [27], that solution may represent a suitable starting point to study a barycentric KS-like formulation in the context of the restricted three body problem, once the rotating frame assumption is removed. The version presented here regularizes the evolution of the physical time based on the distance from the barycenter, but keeps the inertial reference. The proposed barycentric formulation can be extended to a fully Hamiltonian system, if expressed as a doubled set of first order equations, and would be equivalent to the complete Hamiltonian set introduced by Breiter and Langner [26] upon extension to the conjugate momentum of the physical time t. In their derivation, Breiter and Langner exploit a zero-energy manifold for the full Hamiltonian to define the conjugate momentum U^*. The equations of motion are then derived from a new Hamiltonian obtained by applying the Sundman time transformation. The process to extend the barycentric equations of motion to a fully Hamiltonian formulation would be equivalent.

Other works are tailored to the exploration of the most numerical side of the formulation. An extensive analysis of this kind on the KS1 case was proposed by Arakida and Fukushima [37]. Fukushima alone published a series of works that aim to improve the numerical performances of the integration in KS variables and regularized time [38–43]. Several aspects that all contributed to the enhancement of the pure numerical efficiency of the integration were touched: single and quadruple scaling techniques to each of the KS coordinates are proposed, and the latter was extended applying a linear transformation to obtain quasi-conserved quantities to monitor and adjust the scaling during the integration. A time element formulation that reduces the error growth was studied, and then extended to a complete set of variables through the variation of parameters approach. Still within the context of regularized formulation but without using the KS formulation, an orbital longitude integration and manifold correction methods were proposed.

Other works have developed a formalism stemming from the KS approach, in the attempt to regularize the complete N-body problem. Aarseth and Zare [44] started with the regularization of the three-body problem based on the KS formulation for a configuration considering the two primary binaries, extended shortly after by Heggie [45] for any configuration and having regularized collisions for any pairs. Palmer et al. [46] and Mikkola and Aarseth [47–51] extended Aarseth's approach to a N-body chain regularization technique, together with different implementation solutions for how to switch the chain configuration in case of close encounters and analyses of the numerical performance.

Mikkola and Merrit [52, 53] extended the regularization chain algorithm also to include velocity-dependent perturbation sources, with specific mention to general relativity through the post-Newtonian approximation. Their work strictly involves the simulation of full N-body systems, whereas the proposed adaptation and implementation focuses on the motion of a small particle of negligible mass under the action of the gravitational forces of the N-bodies, as well as other arbitrary perturbations.

For planetary protection applications, reducing the precision of the integration simplifying the physical model might lead to significantly different results because of the accumulated error, especially at the end of the integration span. This makes it necessary to deal with a force model that is as complete as possible, which requires the use of ephemerides data to avoid integrating the N-body problem for faster integrations. In fact, the computational burden is currently the major limitation to the extensive performance of planetary protection analysis. Nowadays, the compliance with the requirements outlined for instance by Kminek et al. [2] is assessed with a Monte Carlo based approach, for each point in the trajectory where the disposal of an object is required. Were a trajectory solution to be discarded, all the Monte Carlo runs would need to be run anew, assessing whether the next candidate complies with the requirements or not, and so on. Improving the computational cost of the planetary protection analysis turns therefore into a reduction of the overall trajectory design development time, as any solution whose compliance with the given requirements needs to be secured benefits from more efficient techniques.

On the application viewpoint, KS coordinates have already been used in a few applications. Hernandez and Akella [54] developed a Lyapunov-based guidance strategy using KS coordinates to target several types of orbit conditions, e.g. specified angular momentum vector, and applied it to the design of low thrust trajectories. Woollands et al. [55] developed a Lambert solver based on KS coordinates and used it to provide a good initial guess to the Picard-Chebyshev numerical integration of the perturbed two-body problem. Sellamuthu and Sharma analysed the J_2, J_3, J_4 terms of Earth's oblateness and the third body luni-solar perturbation when approximated with a Legendre polynomial expansion with KS coordinates [56–58]. Using the equation they obtained, they then implemented an orbital propagator and studied the effects of such perturbations on resident space objects with high perigee and highly eccentric orbits.

This work shows that the adoption of KS coordinates in the barycentric restricted relativistic N-body problem reduces the computational cost of the single simulations, and therefore of the whole planetary protection compliance analysis, without any sacrifice of precision. The sensitivity of the regularized formulation on flyby events is mitigated implementing a dynamic and automatic frame switch to the primary body whenever a close approach is detected, generating new KS coordinates for the permanence within the sphere of influence. Section II summarizes the KS1 formulation for a generic perturbed problem, deriving the equations of motion from the original Cartesian formulation obtaining an incomplete Hamiltonian set that handles the barycentric regularized motion with the same numbers of states as the planetocentric one. Quaternion algebra is extensively used and exploited in the derivations. Section III shortly presents the non-dimensionalization technique adopted in SNAPPshot [8] and introduces the adaptive energy-based

strategy that is needed to implement KS coordinates with the dynamic frame switch for flyby events. Section IV presents the optimization approach that exploits the fibration of the KS1 space to minimize the system's numerical stiffness and in turn the number of integration time steps. Section V presents the numerical performances of the proposed approach in comparison to the standard formulation currently employed in SNAPPshot [8].

II. KS regularization

The Kustaanheimo-Stiefel (KS) formulation rewrites the two body problem as an isotropic*, four-dimensional harmonic oscillator. The conservation of the orbital energy is also introduced, leading to a simple linear ordinary differential equation. The first formulation was proposed indeed by Kustaanheimo and Stiefel [11, 12], and extended the usual Cartesian position vector $\underline{r} = \{r_1, r_2, r_3\}^T$ into a four-vector, by adding the length $r = \sqrt{\underline{r} \cdot \underline{r}}$ as fourth coordinate. The underline notation $\underline{r}$ will be used to stress the difference between three-dimensional Cartesian vectors and the KS four vectors/quaternions, denoted in bold $\mathbf{r}$. Using the initial formulation proposed by Kustaanheimo, the physical coordinates are linked to the spinor regularized coordinates $\mathbf{u} = \{u_1, u_2, u_3, u_4\}^T$ through:

$$\begin{aligned} r_1 &= u_1^2 - u_2^2 - u_3^2 + u_4^2 \\ r_2 &= 2\left(u_1 u_2 - u_3 u_4\right) \\ r_3 &= 2\left(u_1 u_3 + u_2 u_4\right) \\ r &= u_1^2 + u_2^2 + u_3^2 + u_4^2 \end{aligned} \tag{1}$$

later re-arranged in matrix-vector product as

$$\mathbf{r} = \mathbf{L}(\mathbf{u})\mathbf{u} \tag{2}$$

which gives $\mathbf{x} = \{r_1, r_2, r_3, 0\}^T$, with

$$\mathbf{L}(\mathbf{u}) = \begin{bmatrix} u_1 & -u_2 & -u_3 & u_4 \\ u_2 & u_1 & -u_4 & -u_3 \\ u_3 & u_4 & u_1 & u_2 \\ u_4 & -u_3 & u_2 & -u_1 \end{bmatrix} \tag{3}$$

The other key concept is converting the integration time from the physical time t to the fictitious time s, with a first order Sundman transformation [10]:

$$\frac{ds}{dt} = \frac{\beta}{r} e^{\int K dt} \tag{4}$$

with β an arbitrary constant coefficient and K an arbitrary function of position, velocity and time. Setting $\beta = 1$ and

*All the four components oscillate with the same frequency and phase.

$K = 0$ to operate the time transformation, replacing $\mathbf{r} = \mathbf{L}(\mathbf{u})\mathbf{u}$ and its derivatives, the KS transformation converts the Kepler two-body problem

$$\ddot{\mathbf{r}} = -\frac{\mu}{r^3}\mathbf{r} \tag{5}$$

into

$$\mathbf{u}'' = \frac{\epsilon}{2}\,\mathbf{u} \tag{6}$$

where $(\ddot{\cdot})$ and $(\cdot)''$ stand for second t and s derivatives respectively, and ϵ denotes the two-body orbital energy. Because the adopted Sundman regularization is of the first order, for unperturbed orbits the new independent variable s follows the evolution of the eccentric anomaly. The achieved behavior reflects a sort of slow motion movie for the near-pericenter part of the orbit, with smaller physical time steps the closer the trajectory gets to the attractor.

Vivarelli [16] first showed the connection with quaternions, introducing the definition $\mathbf{u}^* = \{u_1, u_2, u_3, -u_4\}^T$ as the "anti-involute" of $\mathbf{u}$, later re-defined as "star conjugate" by Waldvogel [24]. For the sake of conciseness, the notation used by Waldvogel is proposed here.

A. KS regularized formulation using quaternion notation

The position vector $\underline{r}$ of the three-dimensional Cartesian space can be written as a quaternion $\mathbf{r}$ with null k component:

$$\underline{r} = \{r_1, r_2, r_3\}^T \longrightarrow \mathbf{r} = r_1 + ir_2 + jr_3 + k \cdot 0 \tag{7}$$

In the following, quaternions are represented with the scalar part as the first element of the associated four-vector. It can be shown that [24], given a quaternion $\mathbf{u} = u_1 + iu_2 + ju_3 + ku_4$, the mapping

$$\mathbf{r} = \mathbf{u}\mathbf{u}^* \tag{8}$$

produces a quaternion $\mathbf{r}$ with vanishing k component, and with the other components as defined in Equation (1):

$$\begin{aligned} r_1 &= u_1^2 - u_2^2 - u_3^2 + u_4^2 \\ r_2 &= 2\big(u_1u_2 - u_3u_4\big) \\ r_3 &= 2\big(u_1u_3 + u_2u_4\big) \end{aligned} \tag{9}$$

The magnitude of $\mathbf{r}$ can also be written in terms of quaternion operations:

$$r^2 = ||\underline{r}||^2 = |\mathbf{r}|^2 = \mathbf{u}\overline{\mathbf{u}} \tag{10}$$

with $\overline{\mathbf{u}} = u_1 - iu_2 - ju_3 - ku_4$ the standard definition of quaternion conjugate.

Following Waldvogel [24], inheriting the conformality properties of the Levi-Civita mapping can partially fix the degree of freedom left whenever mapping from $\mathbb{R}^3$ to $\mathbb{R}^4$. A constraint is added for the definition of the components of $\mathbf{u}$, and particularly appears as the following differentiation rule for $\mathbf{r}$:

$$d\mathbf{r} = 2\mathbf{u}\ \ d\mathbf{u}^* \tag{11}$$

The fiber defining the mapping from $\mathbb{R}^3$ to $\mathbb{R}^4$ can be parametrized by the angle φ, through a two-step process. First, the unique quaternion with vanishing k component is found:

$$\mathbf{u}|_{\varphi=0} = \frac{\mathbf{r} + |\mathbf{r}|}{\sqrt{2(r_1 + |\mathbf{r}|)}} \tag{12}$$

Then, the whole KS fiber is found through φ as

$$\mathbf{u} = \mathbf{u}|_{\varphi=0}\ \ e^{k\varphi} = \mathbf{u}|_{\varphi=0}(\cos\varphi + k\sin\varphi) \tag{13}$$

which is proved as follows [24]:

$$\mathbf{u}\mathbf{u}^* = \mathbf{u}|_{\varphi=0}\ \ e^{k\varphi}\ \ e^{-k\varphi}\mathbf{u}^*|_{\varphi=0} = \mathbf{u}|_{\varphi=0}\mathbf{u}^*|_{\varphi=0} = \mathbf{r} \tag{14}$$

Denoting with $\dot{(\cdot)}$ the derivative with respect to the physical time, the dynamics of the two-body problem can be equivalently written by the Cartesian three-dimensional coordinate $\underline{r}$ or the quaternion with vanishing k component $\mathbf{r}$:

$$\underline{\ddot{r}} = -\frac{\mu}{r^3}\underline{r} \iff \ddot{\mathbf{r}} = -\frac{\mu}{r^3}\mathbf{r} \tag{15}$$

and the two-body energy can be also written in terms of the quaternion $\mathbf{r}$

$$\frac{1}{2}|\dot{\mathbf{r}}|^2 - \frac{\mu}{r} = \epsilon = \text{const} \tag{16}$$

The fictitious time s is now introduced by the Sundman transformation of Equation (4) [10], which becomes:

$$dt = r\ \ ds; \quad \frac{d(\cdot)}{ds} = (\cdot)' \tag{17}$$

The derivatives with respect to the physical time t become

$$\dot{(\cdot)} = \frac{1}{r}(\cdot)'; \quad \ddot{(\cdot)} = \dot{\left(\frac{1}{r}(\cdot)'\right)} = \frac{1}{r}\left(\frac{1}{r}(\cdot)'\right)' = -\frac{1}{r^3}r'(\cdot)' + \frac{1}{r^2}(\cdot)'' \tag{18}$$

with the dynamics and the energy equations re-written as:

$$\begin{aligned} r\mathbf{r}'' - r'\mathbf{r}' + \mu\mathbf{r} &= 0 \\ \frac{1}{2r^2}|\mathbf{r}'|^2 - \frac{\mu}{r} &= \epsilon \end{aligned} \tag{19}$$

Using Equations (8) and (10), the differentiation rule presented in Equation (11) gives

$$\mathbf{r}' = 2\mathbf{u}\mathbf{u}^{*'}; \quad \mathbf{r}'' = 2\mathbf{u}\mathbf{u}^{*''} + 2\mathbf{u}'\mathbf{u}^{*'}; \quad r' = \mathbf{u}'\overline{\mathbf{u}} + \mathbf{u}\overline{\mathbf{u}}' \tag{20}$$

Replacing the definitions of $\mathbf{r}, \mathbf{r}', \mathbf{r}'', r'$ in the dynamics and energy equations and exploiting the properties of quaternion algebra, Equation (20) becomes:

$$\begin{aligned} 2r\mathbf{u}^{*''} + (\mu - 2|\mathbf{u}'|^2)\mathbf{u}^* &= 0 \\ \mu - 2|\mathbf{u}'|^2 &= -r\epsilon \end{aligned} \tag{21}$$

Finally, the expression of the orbital energy appears in the regularized dynamics equation, leading to the simple four-dimensional harmonic oscillator [24]:

$$\mathbf{u}^{*''} - \frac{\epsilon}{2}\mathbf{u}^* = 0 \Longleftrightarrow \mathbf{u}'' - \frac{\epsilon}{2}\mathbf{u} = 0 \tag{22}$$

B. Perturbed problem

Perturbing physical accelerations $\mathbf{f}$, if written again as a quaternion with vanishing k component, are accounted for simply by an additional non-null term on the right hand side of the equations of motion. The generic perturbed two-body problem becomes

$$\ddot{\mathbf{r}} = -\frac{\mu}{r^3}\mathbf{r} + \mathbf{f}(\mathbf{r}, t) \tag{23}$$

The derivation remains equal to the unperturbed case. Introducing the derivative with respect to the KS time gives

$$r\mathbf{r}'' - r'\mathbf{r}' + \mu\mathbf{r} = r^3\mathbf{f}(\mathbf{r}, t) \tag{24}$$

and using $r = \mathbf{u}\overline{\mathbf{u}}$, after multiplying both sides by $\mathbf{u}^{-1}$ a similar expression to Equation (21) is obtained [24]

$$\begin{aligned} 2r\mathbf{u}^{*''} + (\mu - 2|\mathbf{u}'|^2)\mathbf{u}^* &= r^2\overline{\mathbf{u}}\mathbf{f}(\mathbf{r}, t) \\ \mu - 2|\mathbf{u}'|^2 &= -r\epsilon \end{aligned} \tag{25}$$

Note that the energy ϵ is not necessarily constant in the perturbed case. Replacing the energy expression in the equations of motion and dividing by $2r$ leads to

$$\mathbf{u}^{*''} - \frac{\epsilon}{2}\mathbf{u}^* = \frac{r}{2}\overline{\mathbf{u}}\mathbf{f}(\mathbf{r}, t) \tag{26}$$

The final expression is obtained by taking the star conjugate of both sides:

$$\mathbf{u}'' - \frac{\epsilon}{2}\mathbf{u} = \frac{r}{2}\mathbf{f}(\mathbf{r}, t)\overline{\mathbf{u}}^* \tag{27}$$

Since the physical time t can appear in $\mathbf{f}(\mathbf{r}, t)$ either implicitly or explicitly, it should still be tracked, even though its removal was necessary to reach a simpler form of the equations of motion. Closed form expressions for $t = t(s)$ cannot be found for the perturbed case, whereas s evolves like the eccentric anomaly [24], up to a constant, in the unperturbed two-body problem. However, from Equation (17) the relation $dt/ds = r$ can be used to add the physical time as another state element for numerical integrations accounting for perturbations. The two-body energy ϵ can either be computed at each time step with

$$\epsilon = -\frac{1}{r}\left(\mu - 2|\mathbf{u}'|^2\right) \tag{28}$$

or be added as another state element as well, and its derivatives are defined as:

$$\begin{aligned} \epsilon' &= \underline{r}' \cdot \underline{f}(\underline{r}, t) \\ \dot{\epsilon} &= \dot{\underline{r}} \cdot \underline{f}(\underline{r}, t) \end{aligned} \tag{29}$$

C. Barycentric KS formulation for the full force problem

The original KS formulation of the orbital dynamics requires the reference frame to be centered in one body, that serves both as regularization point and primary attractor for the computation of the orbital energy. However, a more complex dynamics that does not necessarily follow a dominantly two-body trajectory could not benefit from the KS regularization if it was kept in its standard form. Moreover, as it will be shown in Section V, the barycentric formulation of the dynamics builds a more efficient simulation already in the Cartesian form, since tidal terms are not present. Such an efficiency improvement is even more relevant when accounting for relativistic effects, since the N-bodies barycenter is the origin of the reference frame where the Post-Newtonian Einstein-Infeld-Hoffmann equations are derived [59].

Because of this reason, with the purpose of building a simulation setup that remains as general as possible in the cases it can efficiently tackle although still featuring the core benefits of the KS formulation, a barycentric formulation of the KS equations of motion is derived. For the sake of conciseness only the perturbing effects of the N bodies are presented. Other perturbing sources, such as relativistic effects and solar radiation pressure, are not explicitly written, as they would follow the same process to be included in the KS formulation of the dynamics.

Before dealing with the barycentric case and to highlight the differences with respect to the perturbing effects of the N-bodies on the traditional KS formulation, keeping the frame centered on one of the N-bodies brings:

$$\mathbf{u}'' - \frac{\epsilon}{2}\mathbf{u} = -\frac{r}{2}\sum_{\substack{n=1 \\ n\neq n_p}}^{N}\left(\frac{\mu_n(\mathbf{r}-\mathbf{r}_n)}{|\mathbf{r}-\mathbf{r}_n|^3} + \frac{\mu_n\mathbf{r}_n}{|\mathbf{r}_n|^3}\right)\overline{\mathbf{u}}^* \tag{30}$$

with n_p identifying the primary body, included in the definition of the two-body energy ϵ, $\mathbf{r}_n$ and μ_n position vector with respect to the primary and gravitational parameter of the body n, respectively.

A few modifications are required to write the dynamics centered in the barycenter of the N bodies involved. In general, through the regularization, smaller physical time steps are implicitly taken in the proximity of the center of the reference frame. Its correspondence with the main attractor in the Keplerian problem is not necessary, but becomes convenient when combined with the expression for the orbital energy ϵ. In the barycentric case, the state $\mathbf{r}$ does not identify the position with respect to the primary, therefore every single gravitational contribution must be included among the right hand side terms. Equation (19) for the barycentric state becomes:

$$\begin{aligned} r\mathbf{r}'' - r'\mathbf{r}' &= -\sum_{n=1}^{N}\frac{\mu_n(\mathbf{r}-\mathbf{r}_n)}{|\mathbf{r}-\mathbf{r}_n|^3} \\ \frac{1}{2r^2}|\mathbf{r}'|^2 - \sum_{n=1}^{N}\frac{\mu_n}{|\mathbf{r}-\mathbf{r}_n|} &= \epsilon_0 \end{aligned} \tag{31}$$

and introducing the KS variables $\mathbf{u}$

$$\begin{aligned} \mathbf{u}'' &= \frac{|\mathbf{u}'|^2}{r}\mathbf{u} - \frac{r}{2}\sum_{n=1}^{N}\frac{\mu_n(\mathbf{r}-\mathbf{r}_n)}{|\mathbf{r}-\mathbf{r}_n|^3}\overline{\mathbf{u}}^* \\ \frac{2}{r}|\mathbf{u}'|^2 - \sum_{n=1}^{N}\frac{\mu_n}{|\mathbf{r}-\mathbf{r}_n|} &= \epsilon_0 \end{aligned} \tag{32}$$

The energy equation may be included in the dynamics only if accounted as the total energy ϵ_0 of the system. The presented formulation is suitable for fully numerical simulations and any other perturbing effect could be included as done for the effects of the N bodies. The numerical performances are presented in Section V.

To extend the presented barycentric formulation to a complete Hamiltonian set of equations, the process proposed by Breiter and Langner [26] can be followed, with the only difference that the zero-energy manifold should be set on the kinetic contribution alone. This follows the way gravitational forces are treated in the force-based derivation outlined in

this section, since they are all included in the right-hand side term. On the contrary, preserving a body-centric reference frame allows to keep the definition of main and perturbing gravitational potential, leading exactly to the formulation proposed by Breiter and Langner [26].

III. Energy-based nondimensionalization and dynamic frame switch

When numerically simulating any dynamic phenomenon, well posed reference quantities allow the states' magnitude to remain as close as possible to the unity along the trajectory, which may boost the numerical performances of the simulator as the time steps taken can be the largest.

SNAPPshot currently implements static reference quantities, such as the "AU-year" based non-dimensionalization [5] for interplanetary tasks, which takes the astronomical unit and the year as typical length and time scales, l_{ref} and t_{ref} , for the orbital phenomena. As only two out of all the four quantities involved are independent, the reference velocity v_{ref} and gravitational parameter μ_{ref} are derived from them:

$$\begin{aligned} l_{ref} &= AU \\ t_{ref} &= Year \\ v_{ref} &= \frac{l_{ref}}{t_{ref}} \\ \mu_{ref} &= \frac{l_{ref}^3}{t_{ref}^2} \end{aligned} \tag{33}$$

Although simple, this reference choice is not optimal for different reasons. First, the state is well referenced only for near-Earth objects. Secondly, the gravitational parameters are never close to the unity, consequently the primary acceleration will not be close to 1. Only the Sun is represented in an acceptable way, with its gravitational parameter μ equal to 2π because of the relation between the year and Earth's orbital period. Lastly, were any flybys to happen, their characterizing fast dynamics would be excessively different from the non-dimensional time and length scales.

It may be reasonable to introduce another non-dimensionalization strategy, that is not sensitive to either the geometry of the possible unperturbed solution (ellipses or hyperbolas in the weakly perturbed two-body problem) and the primary attractor (the Sun for open interplanetary space or a planet for temporary flybys). Note also that, for interplanetary dominantly two-body trajectories but featuring a close approach, it is impossible to properly catch both events with a single choice. It may then be reasonable to allow for a dynamic frame switch for flyby events, following the approach already presented by Amato et al. [36]. The purpose of the proposed work is only to validate the concept of dynamic frame switch, without trying to identify an optimal switch distance as in [36]. The results shown in Section V will prove that, at least for long term application, the simple definition of sphere of influence does not affect the integration accuracy.

The just made observations lead to the following general non-dimensionalization algorithm, valid for both interplanetary and planetary systems, starting from the dimensional state magnitudes expressed with respect to a known primary (i.e. knowing if that initial state is within or without the sphere of influence of a planet). Particularly, the following steps can be taken each time the reference frame is switched, either for initialization or flyby event. First, the state at the entrance/exit of the sphere of influence is converted into its Cartesian and dimensional representation. Secondly, the center of the reference frame is changed by simple vector summation. Third and last, the state is converted back in the original formulation and is made non-dimensional according to the newly updated reference length, time, velocity and gravitational parameter. The new reference dimensions are defined through a four-step process. μ_{ref} is set equal to either the primary or the equivalent gravitational parameter, for dominantly two-body or multi-body cases respectively. Keeping a general notation to include both the equivalent and primary cases, a reference two-body energy is computed as

$$\epsilon_{ref} = -\frac{\mu_{ref}}{r} + \frac{1}{2}v^2 \tag{34}$$

where r and v refer to position and velocity magnitude in the current reference frame (Sun-centric, planetocentric, or barycentric). ϵ_{ref} is used to set the reference length l_{ref} as the absolute value of the semi-major axis of the fictitious orbit that would arise from μ_{ref} and position and velocity in the current reference frame:

$$l_{ref} = \frac{\mu_{ref}}{2|\epsilon_{ref}|} \tag{35}$$

Finally, the reference time t_{ref} and the reference velocity v_{ref} are obtained from the values μ_{ref} and l_{ref}:

$$\begin{aligned} t_{ref} &= \sqrt{\frac{l_{ref}^3}{\mu_{ref}}} \\ v_{ref} &= \frac{l_{ref}}{v_{ref}} \end{aligned} \tag{36}$$

Note that for closed two-body orbits non-dimensionalized in the presented way the orbital period becomes equal to 2π. The choice should be constrained to the sole principal attractor for flyby events whose dynamics is primarily two-body, so that the typical time and length scales can be properly identified.

IV. Optimal selection of the fibration parameter φ with energy-nondimensional variables

Observing the KS equations of motion (Equations (30) and (32)), it can be noted that their right-hand sides are all multiplied by their corresponding element of the KS position vector. Consequently, in the unperturbed case a null element of the vector $\mathbf{u}$ implies a constant value for the corresponding element of $\mathbf{u}'$ throughout the integration. Thus the same element, initially null, evolves linearly, in contrast to the sinusoidal or hyperbolic behavior of the remaining

elements, depending on the bound or unbound trajectory case. As a consequence, having a null element results in an increased numerical stiffness of the system, because of the significantly different state variations.

Despite this effect remains small even in the case of null element, the degree of freedom left by choosing the fibration parameter can be exploited to optimize the simulation, maximizing the numerical stability to achieved minimized integration steps. Other than restoring a common variation trend among the state elements, the best performance can be achieved by also minimizing the difference among the variation magnitudes. A suitable choice of fibration parameter φ would maximize the minimum magnitude element: all the magnitudes of the remaining elements will be bounded from below and, at the same time, their magnitude will be reduced with respect to the original null-element case, to accommodate for the position constraint of Equation (8).

A. Necessary condition for the optimal selection of φ

First, it should be noted that maximizing (minimizing) the value of any of the elements of both the initial and averaged KS states implies having another element with null magnitude. This can be seen because, for both the initial KS vectors $\mathbf{u}_0(\varphi)$ and $\mathbf{u}_0'(\varphi)$, denoting both cases with $\mathbf{p}(\varphi)$ and the four components with $p_l(\varphi)$, $l = 1, ..., 4$ it holds that

$$\frac{d\mathbf{p}(\varphi)}{d\varphi} = \left\{ - p_4(\varphi), p_3(\varphi), -p_2(\varphi), p_1(\varphi) \right\}^T \tag{37}$$

$dp_l/d\varphi = 0$ is necessary for $p_l(\varphi)$ to be locally maximized or minimized, which implies that one other element of $\mathbf{p}(\varphi)$ must vanish. Note that the pairs of linked elements of $\mathbf{p}(\varphi)$ correspond in the vector position for both $\mathbf{u}_0(\varphi)$ and $\mathbf{u}_0'(\varphi)$. Therefore, the same claim holds for initial, period-average and the generic interval-averaged KS states, for both bound and unbound trajectories, because these are simple linear combinations of $\mathbf{u}_0(\varphi)$ and $\mathbf{u}_0'(\varphi)$ in the KS formulation.

Based on this observation, it can be proved that if the magnitude of the minimum magnitude element of both the initial and the averaged KS state vectors is maximized, then that specific φ^* makes that magnitude equal to the magnitude of another of the elements of the same vector. Recalling the collective notation $\mathbf{p}(\varphi)$ for both the cases of $\mathbf{u}_0(\varphi)$ and $\mathbf{u}_0'(\varphi)$, this happens because any element of $\mathbf{p}(\varphi)$ is a continuous, periodic and bounded function of φ. The magnitudes of its elements always remain within the closed intervals $\left[0, \max |p_l(\varphi)|\right]$, with $l = 1, ..., 4$.

Suppose that $p_l(\varphi^*)$, $l = 1, ..., 4$ is the local minimum magnitude element of $\mathbf{p}(\varphi)$. Because of its definition, $|p_l(\varphi^*)| \leq |p_m(\varphi^*)|$, with $m = 1, ...4$ and $m \neq l$. Introducing the variation δ to φ^*, the local minimum magnitude element at the point $\varphi^* + \delta$ will be identified by comparing all the elements $|p_l(\varphi^* + \delta)|$ and $|p_m(\varphi^* + \delta)|$ with each other, requiring only $m \neq l$.

Because of the periodicity, the value $\varphi^* + \delta$ will always be bounded by 0 and 2π, moreover also $p_l(\varphi^* + \delta)$ will be bounded by 0 and $\max |p_l(\varphi)|$. Therefore, the minimum magnitude element either remains identified by p_l, but at the coordinate $\varphi^* + \delta$, or it switches to another $p_m(\varphi^* + \delta)$, with $m = 1, ..., 4$ and $m \neq l$. The above made observation

ensures that any element of $\mathbf{p}(\varphi)$ cannot reach its maximum magnitude while remaining the minimum magnitude element, because its "dual" will vanish.

Suppose that $\tilde{\varphi} = \varphi^* + \delta^*$ identifies a switch condition, i.e. the point where $|p_l(\tilde{\varphi})| = |p_m(\tilde{\varphi})|$ holds, with $m, l = 1, ..., 4$ and $m \neq l$. Introducing the small displacement ν, assume that the minimum magnitude element switches from p_l to p_m when moving from $\tilde{\varphi} - \nu$ to $\tilde{\varphi} + \nu$. Since p_l and p_m are continuous functions of φ and have continuous derivatives, the switch can happen when $dp_l/d\varphi$ and $dp_m/d\varphi$ have either common or different sign. In the former case, the minimum magnitude element will keep increasing or decreasing, depending on the sign of $dp_m/d\varphi$. In the latter case instead, the minimum magnitude element will be either locally minimized or maximized. Therefore, the condition $|p_l(\tilde{\varphi})| = |p_m(\tilde{\varphi})|$ is necessary, but not sufficient, to locally maximize the minimum magnitude element. In turn, the same condition is also necessary to globally maximize the minimum magnitude element.

The presented necessary optimality condition can be used to evaluate all the possible candidates of φ that maximize the minimum magnitude element of the averaged state vector, and then select the actual maximizer. Within a specified φ interval, at most 28 evaluations of the values of φ making two elements equal in magnitude are needed to check all the candidate points, for the eight-dimensional KS state including position and velocity. Analytic formulas can be easily obtained setting the various equalities among all the state elements, because they are linear on $\sin\varphi$ and $\cos\varphi$. They are not reported for the sake of conciseness.

B. Numerical support to the optimal selection of φ

A numerical analysis of the presented necessary optimality condition is given in Figures 1, 2a and 2b. In Figure 1 1000 different initial KS conditions are simulated starting from evenly spaced values of φ between 0 and 2π, for a 100 year simulation of the asteroids Apophis and $2010\mathrm{RF}_{12}$. Despite a fixed and constant value of φ is not necessarily optimal for all the integration intervals arising from the frame switch, the comparison with the analytic optimal φ for the period averaged KS state obtained from the first initial condition can already prove the optimality of the choice. To better highlight the spikes, the plotted analytic function in Figure 1 is $f(\varphi) = -\log(\min|\overline{p}_l(\varphi)|)$, with $l = 1, ..., 8$, normalized and shifted to be graphically superposed to the numerical results. As expected and well predicted by the analytical spikes, the number of time steps taken increases the smaller the smallest magnitude element of the averaged (i.e. manipulated initial) state vector become. Furthermore the absolute minima for the time steps are well predicted by the points of maximized minimum magnitude element (black envelope line) in Figures 2a and 2b, where the validity of the necessary optimality condition is also confirmed as such points feature two of the vector elements (grey) with equal magnitudes. The small oscillations that can be seen in the simulation results of Figure 1 are due to the chaotic full dynamics being integrated instead of the unperturbed two-body problem, whose magnitude is anyway much smaller than the time step reduction achieved by selecting the optimal φ instead of, for instance, $\varphi = 0$. Choosing the optimal φ is therefore proved to also be a robust choice for always step-wise nearly optimal simulations in the perturbed environment.

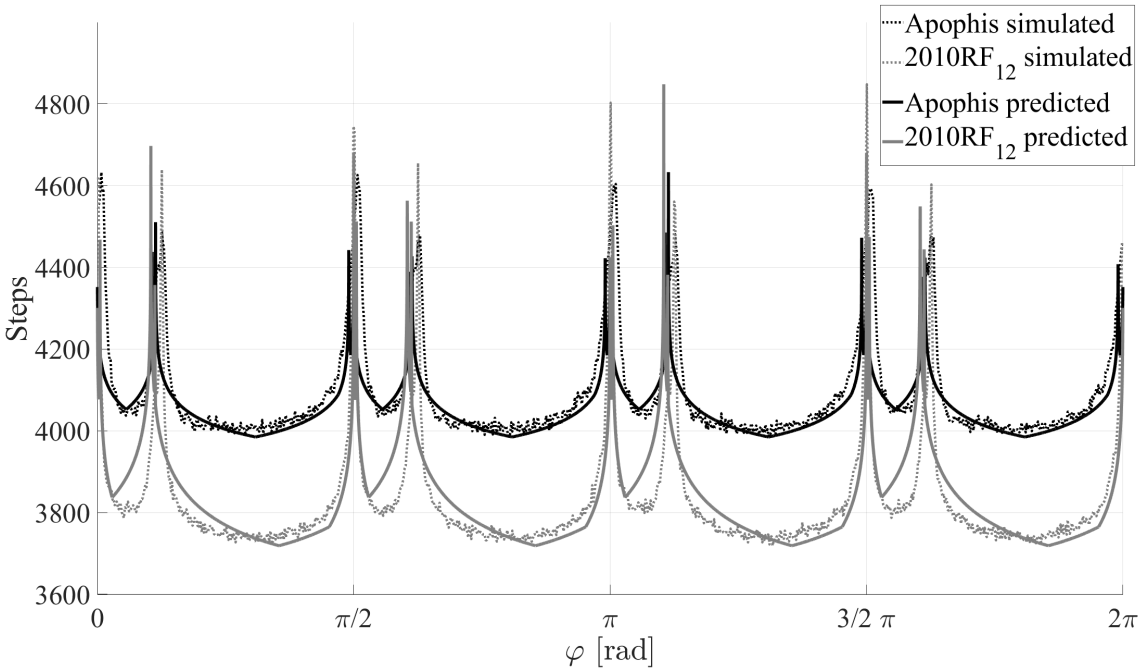

Fig. 1 Time steps dependence on the fibration parameter φ.

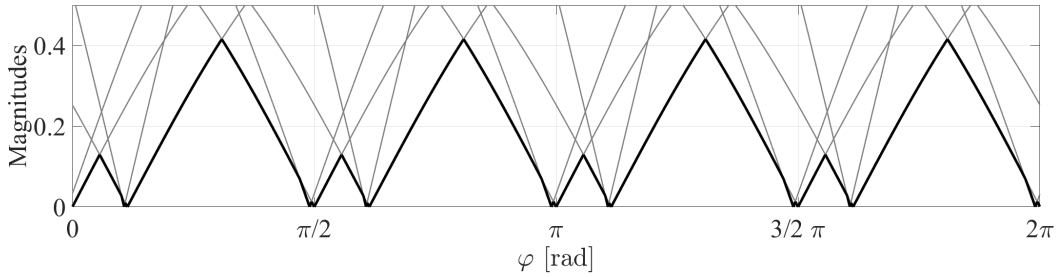

(a) Apophis

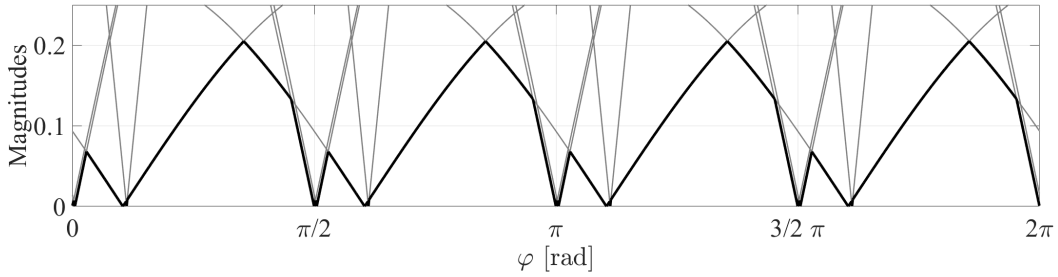

(b) 2010RF$_{12}$

Fig. 2 Non-dimensional magnitude of the minimum magnitude element (black), compared against the magnitude variation of all the KS state elements (grey).

The simulations are performed in the same framework that will be better detailed in Section V, also the evolution of the position error $|\Delta\mathbf{r}| = |\mathbf{r}_{simulation} - \mathbf{r}_{ephemerides}|$ with respect to the ephemerides data for the two asteriods does not change with φ and is always the one presented in Figures 3a and 3b, thus φ can be exploited with the purpose of performing faster simulations.

V. Numerical performances and validation for the single simulation

The performances of the different simulation strategies in the single long term simulation will be shown for the two near Earth asteroids Apophis and 2010RF$_{12}$, in terms of time steps taken, CPU runtime and error evolution with respect to SPICE data. The initial state was taken from SPICE ephemerides data on the 1st January 1989 at noon and the simulations are carried out 100 years forward in time in the J2000 reference frame. Both the asteroids feature a steep close encounter with Earth within this time span. Due to the prevalent interplanetary nature of the motion the integration neglects J_2 and drag effects. Solar radiation pressure is not considered, because the product of the refraction coefficient for asteroids and the area-to-mass ratio is negligible, and also difficult to estimate given the irregular asteroid shapes and variable material composition. General relativity effects are included, based on a self manipulation [60] of the post-Newtonian model proposed by Will [59] as written by Seidelmann [61]. The simulations have been performed using an Intel® Xeon® CPU E5-4620 V4 running at 2.10 GHz.

The following nomenclature is used to identify the tested cases: "FIXED" or "SWITCH" to consider whether switching the integration center in case of flybys, "COWELL" or "KS" for the adopted dynamics formulation (either the Cartesian or the KS formulation of the restricted N-body problem), "EN" or "AUY" for the energy-based and AU-Year non-dimensionalization strategies respectively, "SUN" or "SSB" for the center of the interplanetary legs (either the Sun's center of mass or the Solar System's barycenter).

A. Single trajectory simulation results

All the presented runs have been performed using the Runge Kutta 4/5 and 7/8 numerical schemes. Dimensional simulations are not presented, as the maximum number of time steps, set to 10^5 in this work, is reached before reaching 5% of the time span, also before the flyby events. Given the problem typical magnitudes (10^8 km for positions, 10^1 km/s for velocities) dimensional simulations could likely be made faster if the values for the absolute tolerances were made high enough. The preferred approach is however to use suitable non-dimensionalization procedures, to preserve robustness that high order schemes, such as the Runge Kutta 7/8 used in this work, have for propagations with stringent tolerances. All the presented analyses have been performed using Matlab® and interfacing with JPL's ephemerides data through the SPICE toolkit [62] for retrieving the coordinates of the N bodies, considered as all the Solar System's planets plus the Moon.

The benchmark time steps and runtimes are reported in Table 1.

Table 1 Simulation performance benchmark, AUY-COWELL-FIXED, average of 200 runs.

			RK45		RK78	
Case	**Features**		**Steps**	**Runtime [s]**	**Steps**	**Runtime [s]**
Apophis	**Relativity** **Centre**	No SSB	63218	140.63	7246	34.25
	Relativity **Centre**	No SUN	63118	149.09	7357	34.88
	Relativity **Centre**	Yes SSB	62863	180.61	7187	39.74
	Relativity **Centre**	Yes SUN	62805	193.42	7316	44.24
2010RF$_{12}$	**Relativity** **Centre**	No SSB	59679	134.21	6820	32.29
	Relativity **Centre**	No SUN	59596	142.12	6934	33.72
	Relativity **Centre**	Yes SSB	59664	167.13	6820	37.59
	Relativity **Centre**	Yes SUN	59625	179.14	6929	42.09

The same cases are re-run making use of the energy non-dimensionalization, shown in Table 2. One can already see that, despite the two objects are near-Earth asteroids, the better tuning of the reference quantities already reduces the number of time steps taken and the total runtime by more or less 10% for the correspondent center and force benchmark cases. No significant step and runtime difference was found running the SWITCH case for the same formulation and non-dimensionalization strategy.

Finally, Table 3 shows the time steps and the runtimes obtained using the KS formulation of the energy non-dimensional variables and dynamically switching the centre of the reference frame to the flyby body whenever the propagated object enters a sphere of influence. The proposed KS barycentric formulation is used when the default center of the interplanetary phase is the SSB, whereas the standard perturbed KS formulation is adopted whenever a flyby happens and also for default Sun-centric integrations in the interplanetary phase. The presented steps and runtimes correspond to the fibration point selected according to the optimization presented in Section IV.A, in the interval $[0, \pi/2]$. To this extent, Figures 2a and 2b show the time steps that are obtained for other values of the fibration parameter φ. The runtime is not reported, although it is proportional to the increase in time steps since the dynamics formulation and implementation remains the same.

Simulations in KS coordinates without frame switch are not presented, because the numerical scheme led to the minimum step-size at the moment of close encounter, exceeding the maximum number of steps (10^6) before the end of the integration span although matching the accuracy of the presented cases in the pre-flyby legs. In fact,

Table 2 Simulation performances, EN-COWELL-FIXED, average of 200 runs.

Case	Features		RK45 Steps	RK45 Runtime [s]	RK78 Steps	RK78 Runtime [s]
Apophis	**Relativity** **Centre**	No SSB	58949	133.11	6551	28.82
	Relativity **Centre**	No SUN	58952	140.90	6646	32.51
	Relativity **Centre**	Yes SSB	58579	166.27	6549	37.40
	Relativity **Centre**	Yes SUN	58519	174.61	6637	40.85
2010RF$_{12}$	**Relativity** **Centre**	No SSB	55770	128.99	6287	27.56
	Relativity **Centre**	No SUN	55749	130.62	6404	31.96
	Relativity **Centre**	Yes SSB	55754	160.14	6282	36.04
	Relativity **Centre**	Yes SUN	55727	165.68	6385	39.81

the regularization concept introduced with the KS formulation makes the dynamics sensitive to flyby events, i.e. nearly-singular accelerations, since happening over a non-regularized center.

For all the presented cases the angle φ for the initial KS vector generation has been set according to the necessary optimality condition, searching for the best among the possible $0 < \varphi < \pi/2$ candidates based on the averaged unperturbed KS state, every time the reference frame was switched. Note that the same condition is used for barycentric simulations, because the problem being weakly perturbed and heavily dominated by the Sun makes the difference between barycentric and Sun-centric coordinates small.

It can be clearly seen in Table 3 that the number of time steps taken drops of almost 40% with respect to the benchmark case, and the total runtime of about 30%, comparing the respective force and center cases. This 10% difference bewteen runtime and time step improvements can be explained by the switch events not computed at all in the previous cases. In any case, the improvement brought by the longer time steps that can be safely taken outbalances the advantages to the KS formulation even for cases where the event computation is not necessarily required, despite the extra function evaluations. Another 10% difference is added if the results obtained using the barycentric KS formulation are compared with the Sun-centric benchmark cases for the same force model.

Figures 3a and 3b portrait the evolution of the position error $|\Delta\mathbf{r}| = |\mathbf{r}_{simulation} - \mathbf{r}_{ephemerides}|$ with respect to JPL's ephemerides data [62] for the two different formulations, Cowell's method with the AU-year non-dimensionalization and KS formulation with energy non-dimensionalization and dynamic frame switch. The precision of the frame switch

Table 3 Simulation performances, EN-KS-SWITCH, average of 200 runs.

Case	Features		RK45 Steps	RK45 Runtime [s]	RK78 Steps	RK78 Runtime [s]
Apophis	**Relativity** **Centre**	No SSB	39760	102.68	4025	23.19
	Relativity **Centre**	No SUN	39806	100.73	4423	25.22
	Relativity **Centre**	Yes SSB	39502	123.03	4007	26.89
	Relativity **Centre**	Yes SUN	39500	130.87	4407	31.60
2010RF$_{12}$	**Relativity** **Centre**	No SSB	37479	94.79	3765	21.88
	Relativity **Centre**	No SUN	37449	95.94	4373	24.95
	Relativity **Centre**	Yes SSB	37448	113.59	3782	25.34
	Relativity **Centre**	Yes SUN	37445	123.49	4366	31.35

and the Energy non-dimensionalization was tested on the Cowell's method too, which is not shown because no visible difference with the results from the benchmark (AU-year, no switch) case was found. Similarly, the RK45 and RK78 numerical schemes are equivalent and non-distinguishable in terms of accuracy, although the latter always requires a lower computational effort. It can be clearly seen that the two respective force cases match, with or without accounting for general relativity effects. This already promotes the KS optimized formulation as the simulation method to be always preferred when compared to Cowell's, even for long term simulations in the fully perturbed environment, as it runs significantly faster achieving the same precision for the correspondent force models. Furthermore, as it can also be seen considering the results presented in Table 3, the relativistic integration in KS variables is always faster than the Cowell's N-body integration, allowing for increased precision and reducing the required computational effort.

Figures 4a and 4b still represent the evolution of the position error throughout the integration accounting for relativistic effects, despite showing its relative magnitude with respect to JPL's ephemerides data, and add a comparison with a higher accuracy integration performed on the EN-COWELL-SWITCH case but setting absolute and relative tolerances to 10^{-14} with the RK78 scheme. The denser higher precision solution has been cubic spline-fitted to the already presented integration, particularly before the flyby events precision difference and fitting noise cannot be told apart. On the contrary, after the flyby it can be seen that the integration performed with the KS formulation remains nearly one order of magnitude closer to the higher precision solution. The relative error measure referred to JPL's ephemerides data for the two asteroids highlights again the flyby effect on long term simulations. For the particular case

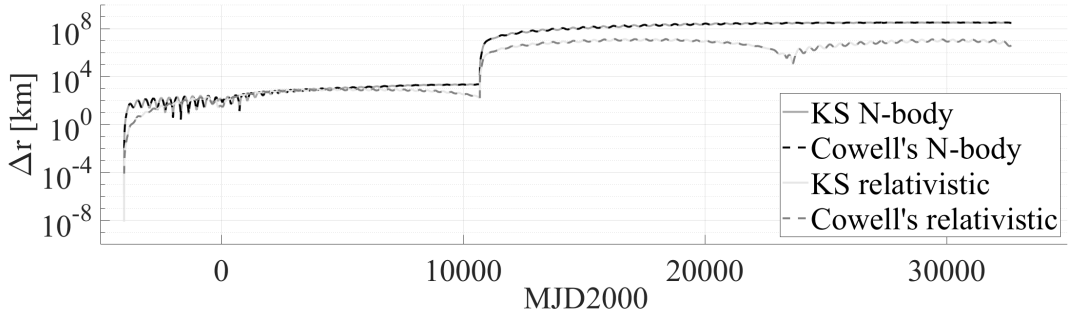

(a) Apophis

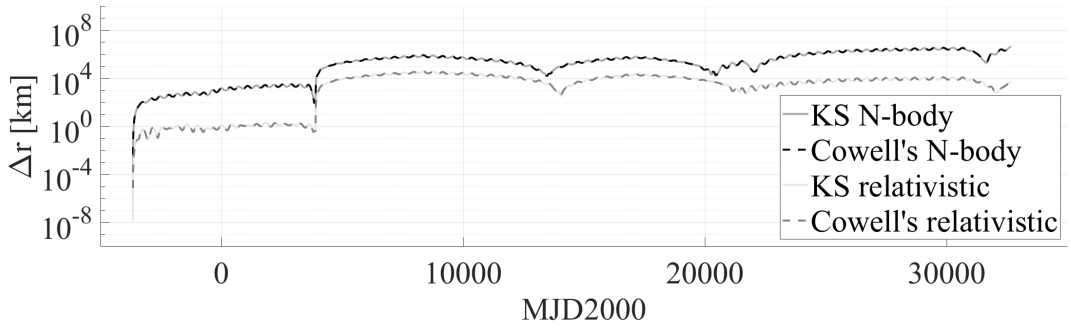

(b) 2010RF$_{12}$

Fig. 3 Position error evolution for the different force models and formulations, with respect to JPL's data.

of Apophis, the steep flyby of Earth has the effect of amplifying by several orders of magnitude the error accumulated before the close encounter. Despite the physical model adopted in this work for the relativistic integration should match the one used by JPL (the user manual points to the model presented by Seidelmann [61] for the ephemerides generation), other error sources are present, which could all explain the still low error accumulated before the flybys: JPL's ephemerides are generated with an Adams-Bashforth scheme and are then stored as coefficient of a polynomial interpolation, so that the user can request their value at specific epochs [62].

B. Monte Carlo simulation and planetary protection analysis in KS coordinates

The case of the upper stage of the launcher of Solar Orbiter (SolO) is presented, performing a Monte Carlo simulation with samples generated from the uncertainty on the initial condition given as a covariance matrix, reported in Table 5 and with initial condition given in Table 4. Such data have been taken from [5], where this test case was studied first. Note that it refers to a mission profile later discarded, whose launch was originally scheduled for late 2018 and ultimately happened in February 2020. The presented results have been obtained with the same simulation routines used for the just discussed single simulation cases.

A total of 54114 samples has been generated for each case and simulated, based on the results of Wilson's expression [63] as done by Jehn [64] and Wallace [65], and following the implementation proposed in [3–5].

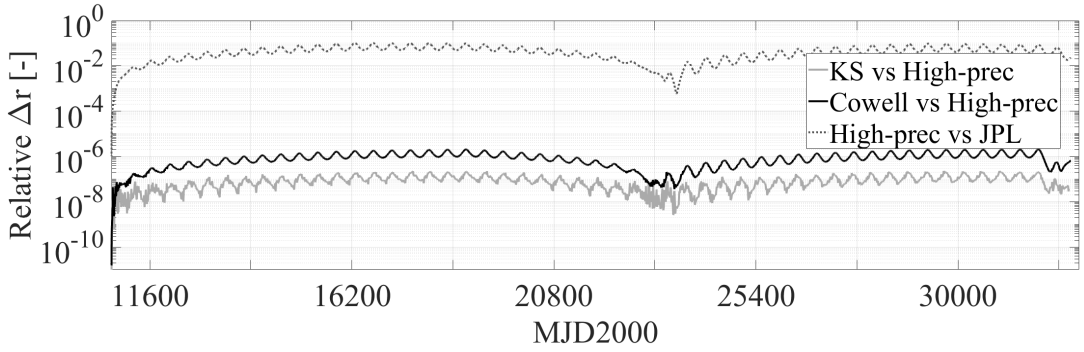

(a) Apophis

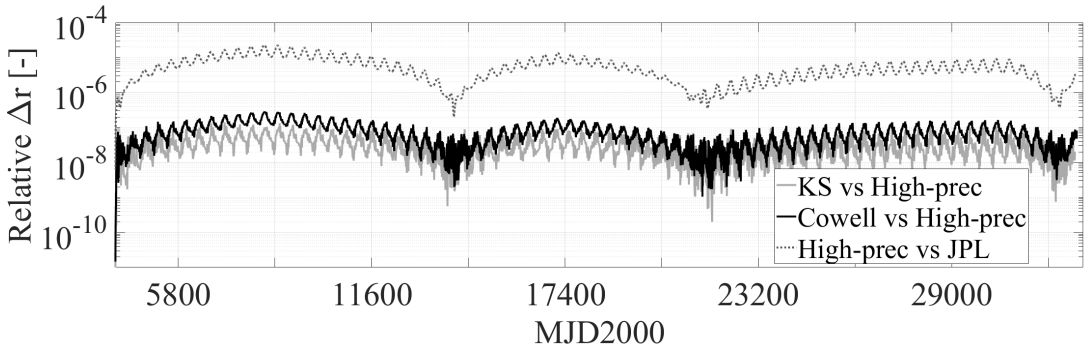

(b) 2010RF$_{12}$

Fig. 4 Relative position error evolution with higher precision relativistic simulation.

Table 4 Inital state of SolO's upper stage of launcher, J2000 reference frame [5].

r_i [km]	r_j [km]	r_k [km]	v_i [km/s]	v_j [km/s]	v_k [km/s]	t_0 [MJD2000]
132048839.02	63140185.88	27571915.38	-12.20	20.24	9.77	6868.62

After the completion of the Monte Carlo simulation, the impact probability of the disposal upper stage of launcher with Earth, Mars and Venus is computed by taking the ratio of the number of simulated impacts over all the generated samples. Tables 6 and 7 presents the results of different Monte Carlo simulations, parallelizing the simulations over 40 cores of the same kind of the one used for the single trajectory simulation. Particularly, the Cowell's case is propagated in one of the two fixed reference frames, SUN and SSB, and persistently checks whether an impact with Venus, Earth and Mars has happened or not at each time step. The KS case switches between either SSB or SUN and planetocentric frames, uses the energy non-dimensionalisation and checks for impacts only if entering any sphere of influence. Also the same numerical scheme, Runge-Kutta 7/8, is used in both cases and for all the samples. In particular, Table 6 highlights the integration steps required by the different setups to detect the impact characterizing the barycenter of the sampled uncertainty cloud. The regularization benefits become particularly visible in this case: impacts can be detected almost twenty times faster, because of the removed mathematical singularity experienced by the Cartesian formulation when approaching any of the considered attractors, and more in general close approaches can be handled by

Table 5 Elements of the covariance matrix of SolO's upper stage of launcher, J2000 reference frame [5].

Position Covariance

	r_i [km]	r_j [km]	r_k [km]
r_i [km]	$5.351\,39 \times 10^{4}$		
r_j [km]	$5.409\,22 \times 10^{4}$	$1.355\,41 \times 10^{5}$	
r_k [km]	$-2.562\,06 \times 10^{4}$	$4.507\,88 \times 10^{3}$	$1.728\,26 \times 10^{5}$

Cross Covariance

	r_i [km]	r_j [km]	r_k [km]
v_i [km/s]	$2.482\,01 \times 10^{-1}$	$2.336\,55 \times 10^{-1}$	$-1.370\,13 \times 10^{-1}$
v_j [km/s]	$2.744\,11 \times 10^{-1}$	$7.100\,15 \times 10^{-1}$	$5.015\,10 \times 10^{-2}$
v_k [km/s]	$-1.205\,15 \times 10^{-1}$	$3.426\,92 \times 10^{-2}$	$8.333\,12 \times 10^{-1}$

Velocity Covariance

	v_i [km/s]	v_j [km/s]	v_k [km/s]
v_i [km/s]	$1.155\,77 \times 10^{-6}$		
v_j [km/s]	$1.179\,08 \times 10^{-6}$	$3.724\,23 \times 10^{-6}$	
v_k [km/s]	$-6.484\,88 \times 10^{-7}$	$3.077\,51 \times 10^{-7}$	$4.019\,29 \times 10^{-6}$

the KS formulation with much larger time steps than what Cowell's method does. The small differences between the barycentric and the Sun-centric results of the barycenter simulation may be due to the particular configuration of the selected case. Table 7 focuses instead on whole Monte carlo outcome. The total runtime is almost halved, achieving a

Table 6 Simulation outcome of the uncertainty barycenter of SolO's upper stage of launcher.

Case	Barycenter	
	Result	Steps
AUY-COWELL-FIXED-SSB	Impact	1872
AUY-COWELL-FIXED-SUN	Impact	1889
EN-COWELL-SWITCH-SSB	Impact	1823
EN-COWELL-SWITCH-SUN	Impact	1798
EN-KS-SWITCH-SSB	Impact	88
EN-KS-SWITCH-SUN	Impact	84

reduction of more than 46%. As the number of time steps taken by the barycenter of the generated cloud (Table 6) tells, this, in turn, provides the observed performance enhancement with respect to the single simulation cases presented in Table 3: estimating impact probabilities requires analyzing what happens close to the encountered bodies, which is also the main advantage of the KS formulation, as it embeds an adaptive scaling of the physical time for different distances from the current primary attractor. Note finally that the estimated impact probability remains basically unchanged, the slight difference might be due to both few borderline cases where the time step that would actually be within the impact

Table 7 Planetary protection analysis of SolO's upper stage of launcher [5]

Case	Estimated impact probability	Runtime
AUY-COWELL-FIXED-SSB	4.0211 %	26.66 hours
AUY-COWELL-FIXED-SUN	4.0211 %	26.45 hours
EN-COWELL-SWITCH-SSB	4.0248 %	27.65 hours
EN-COWELL-SWITCH-SUN	4.0192 %	28.75 hours
EN-KS-SWITCH-SSB	4.0192 %	14.23 hours
EN-KS-SWITCH-SUN	4.0156 %	13.22 hours

region is skipped by the KS integration, and also because of the slightly different samples generated from the initial same covariance matrix (Table 5).

C. Results summary

This work aimed to improve the efficiency of the single simulation strategies, which once performed within a Monte Carlo simulation and post-processed accordingly build a complete planetary protection analysis. Figure 5 shows the relative steps and runtime improvements brought by the different formulations and implementations analyzed in this work, for the single simulations of the asteroids Apophis and $2010RF_{12}$ in the relativistic case, with respect to the AUY-COWELL-FIXED case. The results for the Newtonian simulations that could be plotted from the values available in Tables 1, 2, and 3 are analogous, despite a lower improvement margin introduced by the barycentric simulations.

As dimensional propagations are not efficient in general, the adaptive energy-based non-dimensionalization has been shown to also improve the usual simulation techniques using Cartesian coordinates. For the transition to KS coordinates, this choice of reference quantities becomes necessary, as well as switching the center of reference frame becomes mandatory for the simulation convergence.

The primary-centric KS formulation has been implemented and used in the full force problem and its barycentric counterpart has been derived. In general, the KS approach improves the efficiency of numerical simulations as larger time steps can be taken without any precision loss. Despite the on-paper lost linearity property, the barycentric KS formulation exhibits the best performances overall, both in terms of time steps taken and total runtime required, especially for the relativistic case. In this context, the runtime reduces more than the number of steps, with respect to the KS Sun-centric case. The reduced time steps may be explained by an overall more regular dynamics being propagated, not affected by tidal terms. The further runtime reduction especially evident in relativistic simulations is experienced because evaluating the dynamics function itself is much more efficient in the barycentric case, also being the original frame where the dynamical model is given [61]. Despite not as much as in the relativistic case, an improvement is also obtained in the Newtonian dynamics simulations, again because of the absence if tidal terms in the force model.

The energy-based non-dimensionalization has been exploited to obtain a closed form expression for the optimal

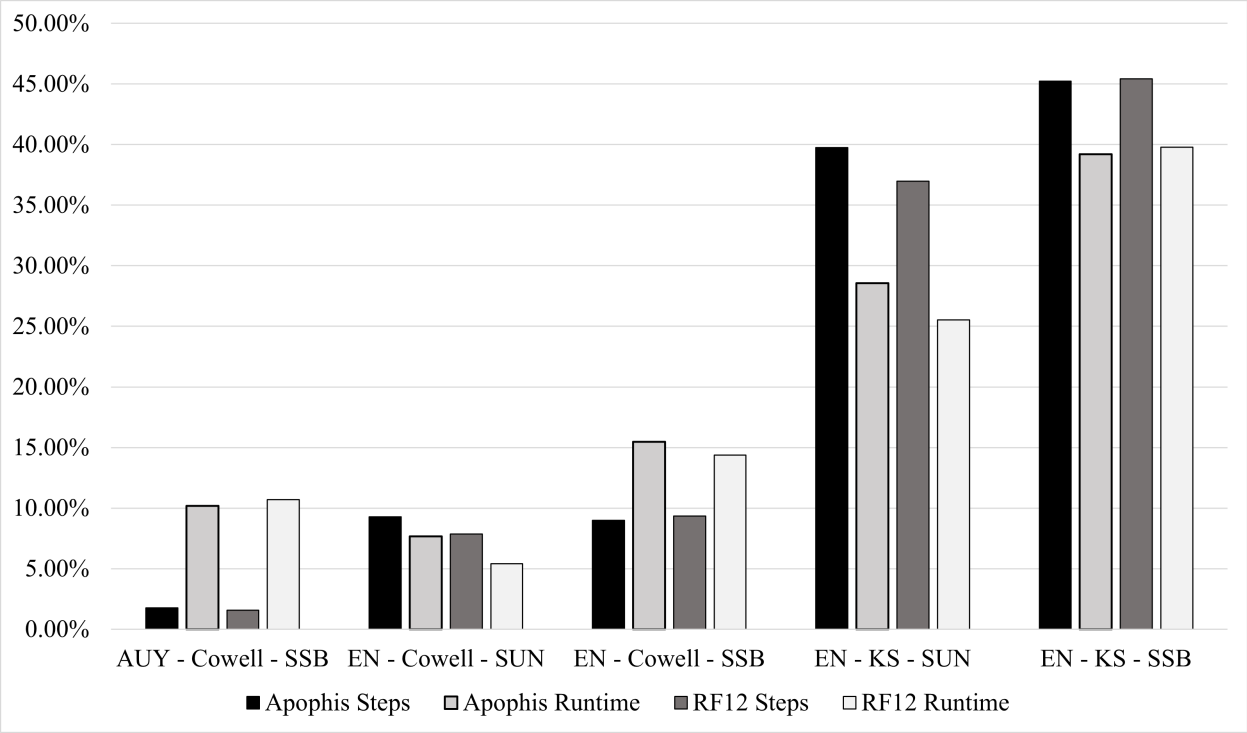

Fig. 5 Speedup provided by the different formulations and implementations.

pre-processing of the KS initial condition, for problems whose primary dynamics remains two-body. The degree of freedom left in the mapping to the four-dimensional KS space has been fixed maximizing the magnitude of the averaged (or initial, equivalently) minimum magnitude element in the unperturbed problem. Because of the way adaptive numerical integration schemes take the initial time steps, the ranges of possible initial conditions that lead to minimized integration steps could be accurately predicted. Furthermore, the improvement is not limited to the step and runtime reduction: as Figures 4a and 4b show, the simulations performed with the KS formulation remain nearly one order of magnitude more accurate than the correspondent Cartesian cases, for the same numerical scheme and absolute and relative integration tolerances.

The proposed KS formulation has been finally adopted to perform the planetary protection analysis of Solar Orbiter's upper stage of launcher. An even larger relative reduction of the total runtime is obtained, with respect to the presented single simulation cases: impacts, therefore close approaches, are the objective of analysis and the KS formulation is exactly built to better handle small distances from the primary. This aspect was highlighted particularly by the much lower time steps taken by the impacting barycenter, it can be seen in Table 6, more than twenty times lower than the usual Cowell's approach.

VI. Conclusions

Kustaanheimo-Stiefel variables have been proven to efficiently propagate trajectories experiencing near singularities, such as flybys or impacts. Implementing a dynamic frame switch procedure was crucial to this extent, shifting also the regularization over the closely approached body. The energetic non-dimensionalization contributes to the overall stability and efficiency of the system, enhancing the numerical performance as the reference quantities it identifies are as close as it can be predicted to the actual trajectory. The barycentric version of the equation of motion ensures the best performance overall because it embeds a dynamical system that is deprived of all tidal terms and therefore made the more regular possible. This version of the dynamics should be tested on low energy problems, to assess whether the same benefits observed on dominantly two-body cases can be obtained on low energy problems or not. The degree of freedom left by the introduction of the fourth dimension in the KS space can be effectively exploited to minimize the numerical stiffness of the system. One possible fibration paradigm exploitation is therefore defined, allowing to identify specific KS states with the purpose of maximizing the efficiency of trajectory propagations.

Single simulations performed in KS coordinates, even if characterized by flybys, experience a reduction of the computational burden of more than 40%, while at the same time remaining nearly one order of magnitude more accurate than the same case propagated in Cartesian coordinates, on a Sun-centric reference frame and with Astronomical Unit and Year set as reference dimensions. Even the highest fidelity tasks, main reason for which most applied simulators using complex force models still use Cartesian coordinates, should be executed in KS coordinates, since their adoption would only bring precision and efficiency advantages.

Finally, it can be said that the more singular the analysis requiring orbital propagations, the greater the improvements that the KS formulation can bring with respect to the Cartesian case, regardless the physical model adopted. The faster assessment of impacts remarkably simplifies one of the computational challenges of the design of mission trajectories. The compliance of a disposal maneuver with planetary protection requirements can be verified almost twice as fast with KS coordinates, without any sacrifice of precision, at least for dominantly two-body trajectory legs. Upon testing of the barycentric version on more modern missions arising from the exploitation of low-energy environments, even in the case of three body-like trajectories the regularization benefits could be introduced, ultimately leading to a generic and efficient computational tool that could contribute to speed-up the trajectory development process.

Funding Sources

The research leading to these results has received funding from the European Research Council (ERC) under the European Union's Horizon 2020 research and innovation programme as part of project COMPASS (Grant agreement No 679086), `www.compass.polimi.it`.

References

[1] COSPAR - Committee on Space Research, "COSPAR Policy on Planetary Protection," *Space Research Today*, Vol. 208, 2020, pp. 10–22. https://doi.org/10.1016/j.srt.2020.07.009.

[2] Kminek, G., "ESA planetary protection requirements, Technical Report ESSB-ST-U-001," Tech. rep., European Space Agency, 2012.

[3] Letizia, F., Colombo, C., Van den Eynde, J., Armellin, R., and Jehn, R., "SNAPPSHOT: Suite for the numerical analysis of planetary protection," *6th International Conference on Astrodynamics Tools and Techniques (ICATT)*, Darmstadt, Germany, 2016.

[4] Letizia, F., Colombo, C., Van den Eynde, J., and Jehn, R., "B-plane visualisation tool for uncertainty evaluation," *Advances in the Astronautical Sciences*, Vol. AAS 16-438, Univelt Inc., Napa, CA, USA, 2016.

[5] Colombo, C., Letizia, F., and Van Der Eynde, J., "SNAPPshot ESA planetary protection compliance verification software Final report V1.0, Technical Report ESA-IPL-POM-MB-LE-2015-315," Tech. rep., University of Southampton, 2016.

[6] Romano, M., Losacco, M., Colombo, C., and Di Lizia, P., "Impact probability computation of near-Earth objects using Monte Carlo line sampling and subset simulation," *Celestial Mechanics and Dynamical Astronomy*, Vol. 132, No. 8, 2020, p. 42. https://doi.org/10.1007/s10569-020-09981-5.

[7] Romano, M., "Orbit propagation and uncertainty modelling for planetary protection compliance verification," Ph.D. thesis, Politecnico di Milano, Supervisors: Colombo, Camilla and Sánchez Pérez, José Manuel, Feb 2020. https://doi.org/10.13140/RG.2.2.19692.80001.

[8] Colombo, C., Romano, M., and Masat, A., "SNAPPshot ESA planetary protection compliance verification software Final report V 2.0, Technical Report ESA-IPL-POM-MB-LE-2015-315," Tech. rep., Politecnico di Milano, 2020.

[9] Kustaanheimo, P., *Spinor Regularization of the Kepler Motion*, 1, Turun Yliopisto, 1964.

[10] Sundman, K. F., "Mémoire sur le problème des trois corps," *Acta Mathematica*, Vol. 36, 1913, pp. 105 – 179. https://doi.org/10.1007/BF02422379.

[11] Kustaanheimo, P., Schinzel, H., and Stiefel, E., "Perturbation theory of Kepler motion based on spinor regularization," *Journal fur die reine und angewandte Mathematik*, Vol. 1965, No. 218, 1965, pp. 204–219. https://doi.org/10.1515/crll.1965.218.204.

[12] Stiefel, E. L., and Scheifele, G., *Linear and Regular Celestial Mechanics*, Grundlehren der mathematischen Wissenschaften, Springer, Berlin, 1971.

[13] Bond, V. R., "The uniform, regular differential equations of the KS transformed perturbed two-body problem," *Celestial mechanics*, Vol. 10, No. 3, 1974, pp. 303–318. https://doi.org/10.1007/BF01586860.

[14] Velte, W., "Concerning the regularizing KS-transformation," *Celestial mechanics*, Vol. 17, No. 4, 1978, pp. 395–403. https://doi.org/10.1007/BF01228959.

[15] Vivarelli, M. D., "The KS-transformation in hypercomplex form and the quantization of the negative-energy orbit manifold of the Kepler problem," *Celestial mechanics*, Vol. 36, No. 4, 1985, pp. 349–364. https://doi.org/10.1007/BF01227489.

[16] Vivarelli, M. D., "Geometrical and physical outlook on the cross product of two quaternions," *Celestial mechanics*, Vol. 41, No. 1, 1987, pp. 359–370. https://doi.org/10.1007/BF01238771.

[17] Vivarelli, M. D., "The Kepler problem: a unifying view," *Celestial Mechanics and Dynamical Astronomy*, Vol. 60, No. 3, 1994, pp. 291–305. https://doi.org/10.1007/BF00691898.

[18] Deprit, A., Elipe, A., and Ferrer, S., "Linearization: Laplace vs. Stiefel," *Celestial Mechanics and Dynamical Astronomy*, Vol. 58, No. 2, 1994, pp. 151–201. https://doi.org/10.1007/BF00695790.

[19] Deprit, A., "The Lissajous transformation I. Basics," *Celestial Mechanics and Dynamical Astronomy*, Vol. 51, No. 3, 1991, pp. 201–225. https://doi.org/10.1007/BF00051691.

[20] Deprit, A., and Elipe, A., "The Lissajous transformation II. Normalization," *Celestial Mechanics and Dynamical Astronomy*, Vol. 51, No. 3, 1991, pp. 227–250. https://doi.org/10.1007/BF00051692.

[21] Deprit, A., and Williams, C. A., "The Lissajous transformation IV. Delaunay and Lissajous variables," *Celestial Mechanics and Dynamical Astronomy*, Vol. 51, No. 3, 1991, pp. 271–280. https://doi.org/10.1007/BF00051694.

[22] Breiter, S., and Langner, K., "The extended Lissajous–Levi-Civita transformation," *Celestial Mechanics and Dynamical Astronomy*, Vol. 130, No. 10, 2018, p. 68. https://doi.org/10.1007/s10569-018-9862-4.

[23] Breiter, S., and Langner, K., "The Lissajous–Kustaanheimo-Stiefel transformation," *Celestial Mechanics and Dynamical Astronomy*, Vol. 131, No. 2, 2019, p. 9. https://doi.org/10.1007/s10569-019-9887-3.

[24] Waldvogel, J., "Quaternions and the perturbed Kepler problem," *Celestial Mechanics and Dynamical Astronomy*, Vol. 95, No. 1, 2006, pp. 201–212. https://doi.org/10.1007/s10569-005-5663-7.

[25] Saha, P., "Interpreting the Kustaanheimo–Stiefel transform in gravitational dynamics," *Monthly Notices of the Royal Astronomical Society*, Vol. 400, No. 1, 2009, p. 228–231. https://doi.org/10.1111/j.1365-2966.2009.15437.x.

[26] Breiter, S., and Langner, K., "Kustaanheimo-Stiefel transformation with an arbitrary defining vector," *Celestial Mechanics and Dynamical Astronomy*, Vol. 128, No. 2, 2017, pp. 323–342. https://doi.org/10.1007/s10569-017-9754-z.

[27] Langner, K., and Breiter, S., "KS variables in rotating reference frame. Application to cometary dynamics," *Astrophysics and Space Science*, Vol. 357, No. 2, 2015, p. 153. https://doi.org/10.1007/s10509-015-2384-6.

[28] Roa, J., and Peláez, J., "Orbit propagation in Minkowskian geometry," *Celestial Mechanics and Dynamical Astronomy*, Vol. 123, No. 1, 2015, pp. 13–43. https://doi.org/10.1007/s10569-015-9627-2.

[29] Roa, J., Urrutxua, H., and Peláez, J., "Stability and chaos in Kustaanheimo–Stiefel space induced by the Hopf fibration," *Monthly Notices of the Royal Astronomical Society*, Vol. 459, No. 3, 2016, p. 2444–2454. https://doi.org/10.1093/mnras/stw780.

[30] Roa, J., and Kasdin, N. J., "Alternative Set of Nonsingular Quaternionic Orbital Elements," *Journal of Guidance, Control, and Dynamics*, Vol. 40, No. 11, 2017, pp. 2737–2751. https://doi.org/10.2514/1.G002753.

[31] Peláez, J., Hedo, J. M., and de Andrés, P. R., "A special perturbation method in orbital dynamics," *Celestial Mechanics and Dynamical Astronomy*, Vol. 97, No. 2, 2007, pp. 131–150. https://doi.org/10.1007/s10569-006-9056-3.

[32] Urrutxua, H., Sanjurjo-Rivo, M., and Peláez, J., "DROMO propagator revisited," *Celestial Mechanics and Dynamical Astronomy*, Vol. 124, No. 1, 2016, pp. 1–31. https://doi.org/10.1007/s10569-015-9647-y.

[33] Baù, G., Bombardelli, C., Peláez, J., and Lorenzini, E., "Non-singular orbital elements for special perturbations in the two-body problem," *Monthly Notices of the Royal Astronomical Society*, Vol. 454, No. 3, 2015, pp. 2890–2908. https://doi.org/10.1093/mnras/stv2106.

[34] Roa, J., Sanjurjo-Rivo, M., and Peláez, J., "Singularities in DROMO formulation. Analysis of deep flybys," *Advances in Space Research*, Vol. 56, No. 3, 2015, pp. 569–581. https://doi.org/10.1016/j.asr.2015.03.019.

[35] Baù, G., and Roa, J., "Uniform formulation for orbit computation: the intermediate elements," *Celestial Mechanics and Dynamical Astronomy*, Vol. 132, No. 2, 2020, p. 10. https://doi.org/10.1007/s10569-020-9952-y.

[36] Amato, D., Baù, G., and Bombardelli, C., "Accurate orbit propagation in the presence of planetary close encounters," *Monthly Notices of the Royal Astronomical Society*, Vol. 470, No. 2, 2017, pp. 2079–2099. https://doi.org/10.1093/mnras/stx1254.

[37] Arakida, H., and Fukushima, T., "Long-Term Integration Error of Kustaanheimo-Stiefel Regularized Orbital Motion. II. Method of Variation of Parameters," *The Astronomical Journal*, Vol. 121, No. 3, 2001, pp. 1764–1767. https://doi.org/10.1086/319408.

[38] Fukushima, T., "Efficient Integration of Highly Eccentric Orbits by Quadruple Scaling for Kustaanheimo-Stiefel Regularization," *The Astronomical Journal*, Vol. 128, No. 6, 2004, pp. 3108–3113. https://doi.org/10.1086/425630.

[39] Fukushima, T., "Efficient Integration of Highly Eccentric Orbits by Scaling Methods Applied to Kustaanheimo-Stiefel Regularization," *The Astronomical Journal*, Vol. 128, No. 6, 2004, pp. 3114–3122. https://doi.org/10.1086/425553.

[40] Fukushima, T., "Efficient Orbit Integration by Kustaanheimo-Stiefel Regularization Using Time Element," *The Astronomical Journal*, Vol. 129, No. 3, 2005, pp. 1746–1754. https://doi.org/10.1086/427718.

[41] Fukushima, T., "Efficient Orbit Integration by Orbital Longitude Methods with Sundmann Transformation on the Time Variable," *The Astronomical Journal*, Vol. 129, No. 2, 2005, pp. 1171–1177. https://doi.org/10.1086/427139.

[42] Fukushima, T., "Efficient Orbit Integration by Linear Transformation for Kustaanheimo-Stiefel Regularization," *The Astronomical Journal*, Vol. 129, No. 5, 2005, pp. 2496–2503. https://doi.org/10.1086/429546.

[43] Fukushima, T., "Efficient Orbit Integration by Manifold Correction Methods," *Annals of the New York Academy of Sciences*, Vol. 1065, No. 1, 2005, pp. 37–43. https://doi.org/10.1196/annals.1370.026.

[44] Aarseth, S. J., and Zare, K., "A regularization of the three-body problem," *Celestial mechanics*, Vol. 10, No. 2, 1974, pp. 185–205. https://doi.org/10.1007/BF01227619.

[45] Heggie, D. C., "A global regularisation of the gravitational N-body problem," *Celestial mechanics*, Vol. 10, No. 2, 1974, pp. 217–241. https://doi.org/10.1007/BF01227621.

[46] Palmer, P. L., Aarseth, S. J., Mikkola, S., and Hashida, Y., "High Precision Integration Methods for Orbit Propagation," *The Journal of the Astronautical Sciences*, Vol. 46, No. 4, 1998, pp. 329–342. https://doi.org/10.1007/BF03546385.

[47] Mikkola, S., and Aarseth, S. J., "A chain regularization method for the few-body problem," *Celestial Mechanics and Dynamical Astronomy*, Vol. 47, No. 4, 1989, pp. 375–390. https://doi.org/10.1007/BF00051012.

[48] Mikkola, S., and Aarseth, S. J., "An implementation of N-body chain regularization," *Celestial Mechanics and Dynamical Astronomy*, Vol. 57, No. 3, 1993, pp. 439–459. https://doi.org/10.1007/BF00695714.

[49] Mikkola, S., and Aarseth, S. J., "A slow-down treatment for close binaries," *Celestial Mechanics and Dynamical Astronomy*, Vol. 64, No. 3, 1996, pp. 197–208. https://doi.org/10.1007/BF00728347.

[50] Mikkola, S., and Aarseth, S. J., "An efficient integration method for binaries in N-body simulations," *New Astronomy*, Vol. 3, No. 5, 1998, pp. 309–320. URL https://www.sciencedirect.com/science/article/pii/S1384107698000189.

[51] Mikkola, S., and Aarseth, S., "A Time-Transformed Leapfrog Scheme," *Celestial Mechanics and Dynamical Astronomy*, Vol. 84, No. 4, 2002, pp. 343–354. https://doi.org/10.1023/A:1021149313347.

[52] Mikkola, S., and Merritt, D., "Algorithmic regularization with velocity-dependent forces," *Monthly Notices of the Royal Astronomical Society*, Vol. 372, No. 1, 2006, pp. 219–223. https://doi.org/10.1111/j.1365-2966.2006.10854.x.

[53] Mikkola, S., and Merritt, D., "Implementing few-body algorithmic regularization with post-Newtonian terms," *The Astronomical Journal*, Vol. 135, No. 6, 2008, pp. 2398–2405. https://doi.org/10.1088/0004-6256/135/6/2398.

[54] Hernandez, S., and Akella, M. R., "Energy preserving low-thrust guidance for orbit transfers in KS variables," *Celestial Mechanics and Dynamical Astronomy*, Vol. 125, No. 1, 2016, pp. 107–132. https://doi.org/10.1007/s10569-016-9677-0.

[55] Woollands, R. M., Read, J., Hernandez, K., Probe, A., and Junkins, J. L., "Unified Lambert Tool for Massively Parallel Applications in Space Situational Awareness," *Journal of the Astronautical Sciences*, Vol. 65, No. 1, 2018, pp. 29–45. https://doi.org/10.1007/s40295-017-0118-4.

[56] Sellamuthu, H., and Sharma, R. K., "Orbit Theory with Lunar Perturbation in Terms of Kustaanheimo–Stiefel Regular Elements," *Journal of Guidance, Control, and Dynamics*, Vol. 40, No. 5, 2017, pp. 1272–1277. https://doi.org/10.2514/1.G002342.

[57] Sellamuthu, H., and Sharma, R. K., "Hybrid Orbit Propagator for Small Spacecraft Using Kustaanheimo–Stiefel Elements," *Journal of Spacecraft and Rockets*, Vol. 55, No. 5, 2018, pp. 1282–1288. https://doi.org/10.2514/1.A34076.

[58] Sellamuthu, H., and Sharma, R. K., "Regularized luni-solar gravity dynamics on resident space objects," *Astrodynamics*, Vol. 5, No. 2, 2020, pp. 91–108. https://doi.org/10.1007/s42064-020-0085-6.

[59] Will, C. M., *Theory and Experiment in Gravitational Physics*, 2nd ed., Cambridge University Press, 2018. https://doi.org/10.1017/9781316338612.

[60] Masat, A., Romano, M., and Colombo, C., "B-plane orbital resonance analysis and applications," Master's thesis, Politecnico di Milano, 2019. URL https://www.diva-portal.org/smash/get/diva2:1440101/FULLTEXT01.pdf.

[61] Seidelmann, P. K., *Explanatory Supplement To The Astronomical Almanac*, University Science Books, 1992.

[62] Acton, C. H., "Ancillary data services of NASA's Navigation and Ancillary Information Facility," *Planetary and Space Science*, Vol. 44, No. 1, 1996, pp. 65–70. https://doi.org/10.1016/0032-0633(95)00107-7.

[63] Wilson, E. B., "Probable Inference, the Law of Succession, and Statistical Inference," *Journal of the American Statistical Association*, Vol. 22, No. 158, 1927, pp. 209–212. URL http://www.jstor.org/stable/2276774.

[64] Jehn, R., "Estimating the impact probability of ariane upper stages," Tech. rep., MAS Working paper 601, European Space Agency, Dec 2014.

[65] Wallace, M., "A Massively Parallel Bayesian Approach to Planetary Protection Trajectory Analysis and Design," *Proceedings of the 2015 AAS/AIAA Astrodynamics Specialist conference*, Vol. AAS 15-535, Vail, CO, USA, 2015. URL https://hdl.handle.net/2014/45859.